Fraction of Boroxol Rings in Vitreous Boron Oxide from a First-Principles Analysis of Raman and NMR Spectra

P. Umari* and Alfredo Pasquarello

Ecole Polytechnique Fédérale de Lausanne (EPFL), Institute of Theoretical Physics, CH-1015 Lausanne, Switzerland
Institut Romand de Recherche Numérique en Physique des Matériaux (IRRMA), CH-1015 Lausanne, Switzerland
(Received 30 March 2005; published 22 September 2005)

We determine the fraction f of B atoms belonging to boroxol rings in vitreous boron oxide through a first-principles analysis. After generating a model structure of vitreous B_2O_3 by first-principles molecular dynamics, we address a large set of properties, including the neutron structure factor, the neutron density of vibrational states, the infrared spectra, the Raman spectra, and the ^{11}B NMR spectra, and find overall good agreement with corresponding experimental data. From the analysis of Raman and ^{11}B NMR spectra, we yield consistently for both probes a fraction f of ~ 0.75. This result indicates that the structure of vitreous boron oxide is largely dominated by boroxol rings.

DOI: 10.1103/PhysRevLett.95.137401 PACS numbers: 78.30.−j, 61.43.Fs, 63.50.+x, 71.15.Mb

The identification of superstructural units in glasses often provides the sole key for understanding the glass structure on length scales extending beyond nearest neighbors. In vitreous B_2O_3, the basic BO_3 triangular units can arrange in planar boroxol rings [1]. However, the fraction f of B atoms in such rings has remained undetermined despite more than four decades of investigations. Analyses of x-ray and neutron diffraction experiments give values of f ranging from 0 to 1 [2–6], suggesting that these experiments are not sufficiently sensitive to restrain the value of f. At variance, experimental techniques which probe the structure only in an indirect way appear potentially more informative. Through isotopic substitution in a Raman scattering study, the sharp line that dominates the spectrum at ~ 800 cm^{-1} could unambiguously be assigned to oxygen motions in boroxol rings [7]. However, an estimate of f remained beyond reach because of the unknown modulation of the Raman intensities. The boroxol peak is also observed in highly resolved inelastic-neutron scattering spectra [5,8], but the estimation of f is hindered by difficulties in separating out the one-phonon scattering contribution. Nevertheless, a comparative study with crystalline polymorphs containing boroxol rings is qualitatively consistent with a high value of f [8]. A particularly sensitive probe to the local structure in vitreous B_2O_3 is NMR [9–11]. The ^{11}B spectrum reveals two sites with relative populations in a ratio of 1:3, from which a value of $f \sim 0.75$ has been derived [10]. However, this assignment cannot be considered as conclusive in absence of a clear understanding of the origin of the NMR shifts. ^{17}O spectra have also been obtained, but their interpretation appears less trivial due to the occurrence of at least three different sites [11].

In this work, we determine the fraction f of B atoms belonging to boroxol rings in vitreous boron oxide through a first-principles analysis. Using first-principles molecular dynamics [12], we first generate a model structure of vitreous B_2O_3 containing boroxol rings. For this model structure, the neutron structure factor, the neutron vibrational density of states, and the infrared spectra are found in excellent agreement with experiment. Using the calculated Raman activities for the vibrational modes in our model, we then derive a value of the fraction f from the experimental intensity of the boroxol peak. Furthermore, we calculate ^{11}B NMR chemical shifts for the generated model structure and provide an interpretation of these shifts in terms of the local geometry. This relation explains the origin of the two peaks in the experimental NMR spectrum and provides firm support to the fraction f inferred from their relative intensities. Both the Raman and NMR analyses consistently fix the value of f at ~ 0.75, thereby removing any residual indetermination concerning the structural units in vitreous B_2O_3.

We generated a model structure of vitreous boron oxide using a first-principles molecular dynamics approach [12,13]. The initial configuration was obtained by adapting the topology of the high-pressure crystalline polymorph B_2O_3-II [15] to a cubic periodic simulation cell. The model consists of 160 atoms at the experimental density of the glass at room temperature (1.83 g/cm^{-3}) [16]. Since the B_2O_3-II structure only contains fourfold coordinated B atoms, it was considered as an unbiased starting configuration for modelling vitreous B_2O_3, in which the B atoms are predominantly threefold coordinated. After a brief thermal spike at high temperature for disrupting the crystalline order, the system was evolved in a diffusive regime for 17 ps at temperatures ranging between 2000 and 3000 K. Then, a gradual quench over a period of 6 ps yielded the present model. We stress that the quench rate in the simulation is orders of magnitude faster than in typical experimental conditions. Hence, one should not expect that our simulation bears the right fraction of boroxol rings

 © 2005 The American Physical Society

[17], but rather that the obtained model structure could prove useful in the interpretation of experimental data [17,18].

The resulting structure consists of a regular network of corner-sharing BO_3 units with only two overcoordinated atoms, which were found not to affect any of the results in the following. The model shows an average bond length of 1.38 Å, in excellent agreement with the experimental value of 1.37 Å [4]. For the BO_3 units, we found an O-B-O angle of $120.0° \pm 3.3°$, implying highly planar and regular configurations. The B-O-B angle distribution has an average value of 133.5° and a spread of 9.6°. An outstanding feature of our model is the occurrence of two noncontiguous boroxol rings. These rings feature very regular structural properties, showing a high planarity with a B-O-B angle of $119.7° \pm 0.5°$. The planarity is further demonstrated through the sums of all bond angles in the rings, which give 717.2° and 718.4°, very close to the ideal value of 720°. The average B-O-B angle for O atoms not belonging to boroxol rings is $134.4° \pm 9.2°$. The comparison in Fig. 1 between the calculated and measured static neutron structure factor [5] shows an excellent agreement for the full range of transferred momenta Q. In particular, a good agreement is also found for the first sharp diffraction peak at $Q = 1.6$ Å^{-1}, which arises from the intermediate range order in the vitreous structure. However, this agreement does not guarantee that the concentration of boroxol rings is accurately reproduced in our model, as is inferred from the range of values for the fraction f derived from diffraction measurements [2–6].

The validity of our model also extends to the description of the vibrational properties. We calculated the dynamical matrix numerically by taking finite differences of the atomic forces for atomic displacements of ± 0.1 bohr [13]. The calculated neutron one-phonon density of states [19] shows overall good agreement with the corresponding experimental spectrum [20] (Fig. 2), both for the positions and the intensities of the three main peaks. In this comparison, we adopted the experimental conditions for the energy-dependent resolution and range of transferred momenta. When a higher resolution is used in the theoretical spectrum (not shown), a peak corresponding to the two boroxol rings appears at ~97 meV, in accord with experimental observations [5,8]. However, this feature cannot be used for estimating the fraction f in absence of an experimental calibration of its intensity in the one-phonon vibrational spectrum [5,8].

Further support for the structural and vibrational properties of our model structure comes from the infrared response function $\epsilon(\omega)$ (Fig. 3). Infrared coupling tensors were obtained by numerically calculating first derivatives of the atomic forces with respect to the electric field, using field intensities of ± 0.0005 and ± 0.001 atomic units [13,21,22]. Both the real (ϵ_1) and the imaginary part (ϵ_2) of $\epsilon(\omega)$ calculated for our model structure closely reproduce the positions and relative strengths of the experimental features [23]. We found a similar good agreement for the energy loss function $-\mathrm{Im}[1/\epsilon(\omega)]$ (not shown). In particular, we found LO-TO splittings of 22 and 318 cm^{-1} for the low and high-frequency peaks in $\epsilon_2(\omega)$, in good agreement with the respective experimental values of 20 and 290 cm^{-1}.

The good level of agreement with experiment achieved for the inelastic-neutron and infrared spectra stems from the occurrence of regular structural units (BO_3) in our model and is only poorly informative on the network organization beyond nearest neighbors [19,22,24]. At variance, the Raman spectrum is highly sensitive to the bonding angle on the O atoms, which connect the basic BO_3 units. These properties clearly appeared for vitreous SiO_2 where dramatic changes occurred in the simulated Raman spectrum for models with different angular distributions [17], while the inelastic-neutron and infrared spectra remained only barely affected [19,22,24]. Among the vibrational spectra, the Raman spectrum is therefore expected to be the most sensitive to the fraction f.

Raman coupling intensities were obtained by numerically evaluating second derivatives of the atomic forces with respect to the electric field [13,21,22]. Raman spectra

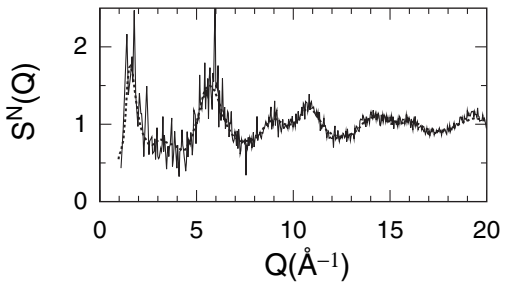

FIG. 1. Static neutron structure factor calculated for the present model structure at a temperature of 15 K (solid line), compared to the experimental structure factor (dashed line) [5]. The theoretical structure factor is calculated for harmonic vibrations [31].

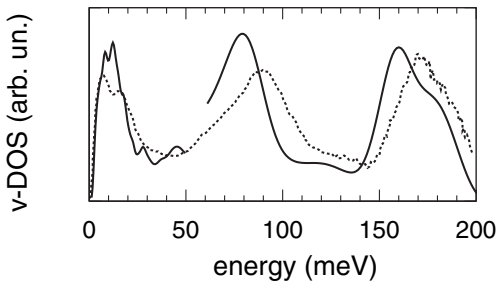

FIG. 2. Neutron density of states calculated for the present model structure (solid line), compared to the experimental spectrum (dashed line) [20]. The experimental spectrum is composed of two parts joined at ~70 meV. The low-frequency and the high-frequency parts were measured at 15 K and at room temperature, respectively. In the theoretical spectrum, the two parts are separately normalized to the integrated experimental intensities in the ranges of 0–50 meV and 70–200 meV.

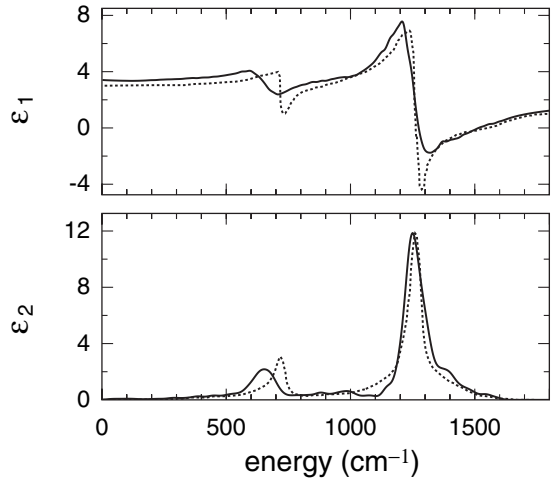

FIG. 3. Real (ϵ_1) and imaginary (ϵ_2) parts of the infrared response function for the present model structure (solid line), compared to the experimental response function (dashed line) [23]. In the theoretical spectra, a Lorentzian and Gaussian broadening of 15 cm^{-1} were applied for ϵ_1 and ϵ_2, respectively.

for our model structure of vitreous B_2O_3 were calculated for incoming and outgoing photons with parallel (HH) and perpendicular polarizations (HV) and compared in Fig. 4 to the corresponding experimental spectra [23]. The agreement between theory and experiment is less impressive than for the other spectroscopies. One observes a clear correspondence between the main frequency bands at 0–300 cm^{-1}, 300–850 cm^{-1}, and 1200–1600 cm^{-1}, but the theoretical spectrum shows a redistribution of the intensities within the two bands of higher frequencies. This is

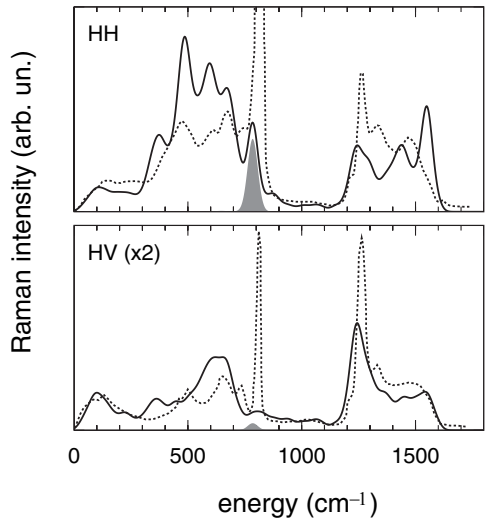

FIG. 4. Reduced HH and HV Raman spectra calculated for the present model structure (solid line), compared to the experimental spectra (dashed line) [23]. The contribution from breathing motions of O atoms in the boroxol rings is highlighted. The calculated spectra are scaled to match the integrated intensity of the experimental HV spectrum. A Gaussian broadening of 22 cm^{-1} is applied.

a preliminary indication that the fraction f in our model (9.4%) significantly differs from the experimental value. The boroxol peak is nonetheless clearly recognizable in the calculated spectra. By projecting the vibrational modes on the in-phase breathing motions of oxygen atoms in the boroxol rings [25], we found a well-defined peak at 786 cm^{-1}, in accord with the experimental boroxol peak at 808 cm^{-1} (Fig. 4) [23]. We calculated a depolarization ratio for this peak of 0.05, to be compared with the experimental value of 0.04 [23]. Furthermore, upon $^{16}O \rightarrow {}^{18}O$ substitution, this peak was found to shift by 42 cm^{-1}, close to the experimental shift of 48 cm^{-1} [7]. The boroxol peak in the theoretical spectra clearly features a weaker intensity than in the experimental spectra.

Despite the nonrepresentative fraction of boroxol rings in our model, we can derive an estimate of f from the experimental spectrum assuming that our calculation accurately reproduces the types of vibrational modes and their coupling factors as a function of frequency [17,26]. Our analysis focuses on the reduced HH Raman spectrum for frequencies up to 1000 cm^{-1}, where the O bending motions occur and are found to dominate the Raman intensity. In our model, their contribution amounts to 84% of the intensity in the considered spectral range, as we could evaluate by projecting the eigenmodes onto the O bending motions prior to the calculation of the Raman intensity [17]. The bending motions of O atoms in boroxol rings account for the prominent boroxol peak, while the other O atoms contribute to the more diffuse background intensity. As indicated by our calculation, it is appropriate to consider different coupling factors for these two kinds of O atoms. The residual contribution to the Raman intensity in the 0–1000 cm^{-1} range results from out-of-plane B vibrations. Hence, we accounted for the contribution of these modes by considering a coupling factor proportional to the total number of atoms (N_{tot}). These assumptions lead us to

$$I_{\mathrm{boroxol}} = \alpha N_{\mathrm{O,boroxol}}, \tag{1}$$

$$I_{\mathrm{backgr.}} = \beta N_{\mathrm{O,nonboroxol}} + \gamma N_{\mathrm{tot}}, \tag{2}$$

where I_{boroxol} and $I_{\mathrm{backgr.}}$ are the integrated HH intensities of the boroxol peak and of the remaining background in the 0–1000 cm^{-1} range, respectively; $N_{\mathrm{O,boroxol}}$, $N_{\mathrm{O,nonboroxol}}$ are the number of O atoms inside and outside the boroxol rings. The ratios β/α and γ/α do not depend on f and could therefore reliably be extracted from our model: $\beta/\alpha = 0.71$ and $\gamma/\alpha = 0.082$. The ratio $I_{\mathrm{boroxol}}/I_{\mathrm{backgr.}}$ is easily inferred from experimental spectra and can now directly be expressed in terms of the fraction f through Eqs. (1) and (2) [27]. Using the experimental spectra from Ref. [23], we arrived at a fraction f of 0.77.

To corroborate the value of f derived from our analysis of the Raman spectrum with an estimate from a different experimental probe, we addressed the origin of ^{11}B NMR chemical shifts. We calculated isotropic ^{11}B chemical

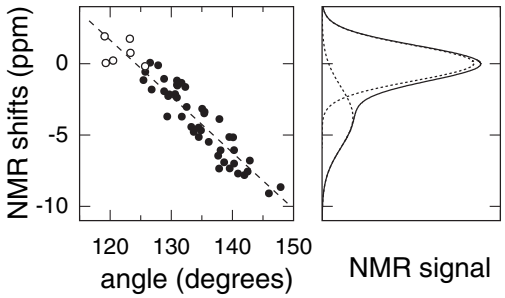

FIG. 5. ^{11}B NMR chemical shifts. Left: Calculated shifts vs mean B-O-B angle for B atoms in the present model structure, belonging (open symbols) or not (solid symbols) to boroxol rings. The dashed line corresponds to the linear regression. The chemical shifts are reported on a relative scale. Right: simulated isotropic NMR spectrum for $f \sim 0.75$.

shifts for our model structure using the scheme of Sebastiani and Parrinello [28]. The calculated shifts are found to depend linearly on the average B-O-B angle (Fig. 5), similarly, as for ^{29}Si chemical shifts in silica polymorphs [29]. This behavior provides a clear interpretation for the origin of two sites in the experimental spectrum. In fact, two kinds of B atoms can be distinguished. Boron atoms in boroxol rings show two B-O-B angles of $\sim 120°$ and a third one as given by the average bond-angle distribution for O atoms not in boroxol rings. At variance, for B atoms not belonging to boroxol rings, the average B-O-B angle only results from the latter bond-angle distribution. To simulate the NMR spectrum of isotropic ^{11}B chemical shifts for the case of $f = 0.75$, we adopted the B-O-B bond-angle distributions as found in our model structure and used the relation determined above between average angle and chemical shift (Fig. 5). The simulated spectrum resembles the experimental one when the quadrupolar term becomes small [10]. In particular, we calculated a separation between the two components of 3.7 ppm, in agreement with the experimental value of 3.6 ± 0.4 ppm [30].

In conclusion, we provided multiple evidences supporting a value of $f \sim 0.75$, indicating that the structure of vitreous B_2O_3 is largely dominated by boroxol rings.

We thank D. Sebastiani for providing helpful assistance. We acknowledge support from the Swiss National Science Foundation (Grant No. 620-57850.99) and the Swiss Center for Scientific Computing.

*Present address: Department of Materials Science and Engineering (DMSE), Massachusetts Institute of Technology (MIT), Cambridge, MA 02139, USA.

[1] J. Krogh-Moe, Phys. Chem. Glasses **6**, 46 (1965).
[2] R. L. Mozzi and B. E. Warren, J. Appl. Crystallogr. **3**, 251 (1970).
[3] S. R. Elliott, Philos. Mag. B **37**, 435 (1978).
[4] P. A. V. Johnson, A. C. Wright, and R. N. Sinclair, J. Non-Cryst. Solids **50**, 281 (1982).
[5] A. C. Hannon *et al.*, J. Non-Cryst. Solids **177**, 299 (1994).
[6] J. Swenson and L. Börjesson, Phys. Rev. B **55**, 11 138 (1997).
[7] C. F. Windisch, Jr. and W. M. Risen, Jr., J. Non-Cryst. Solids **48**, 307 (1982).
[8] R. N. Sinclair *et al.*, Phys. Chem. Glasses **42**, 286 (2000).
[9] G. E. Jellison, Jr., L. W. Panek, P. J. Bray, and G. B. Rouse, Jr., J. Chem. Phys. **66**, 802 (1977).
[10] R. E. Youngman and J. W. Zwanziger, J. Non-Cryst. Solids **168**, 293 (1994).
[11] R. E. Youngman *et al.*, Science **269**, 1416 (1995).
[12] R. Car and M. Parrinello, Phys. Rev. Lett. **55**, 2471 (1985); A. Pasquarello *et al.*, Phys. Rev. Lett. **69**, 1982 (1992); K. Laasonen *et al.*, Phys. Rev. B **47**, 101 42 (1993).
[13] The electronic structure is described within a generalized gradient approximation [14] to density functional theory. We used ultrasoft pseudopotentials for B and O atoms. The electronic wave functions and the charge density are described by plane-wave basis sets with cutoffs of 24 and 250 Ry. The Brillouin zone is sampled at the Γ point.
[14] J. P. Perdew *et al.*, Phys. Rev. B **46**, 6671 (1992).
[15] C. T. Prewitt and R. D. Shannon, Acta Crystallogr. B **24**, 869 (1968).
[16] P. B. Macedo, W. Capps, and T. A. Litowitz, J. Chem. Phys. **44**, 3357 (1966).
[17] P. Umari, X. Gonze, and A. Pasquarello, Phys. Rev. Lett. **90**, 027401 (2003).
[18] A. Pasquarello, Curr. Opin. Solid State Mater. Sci. **5**, 503 (2001).
[19] J. Sarnthein, A. Pasquarello, and R. Car, Science **275**, 1925 (1997); Phys. Rev. B **57**, 14 133 (1998).
[20] A. C. Hannon, R. N. Sinclair, and A. C. Wright, Physica A (Amsterdam) **201**, 375 (1993).
[21] P. Umari and A. Pasquarello, Phys. Rev. Lett. **89**, 157602 (2002).
[22] P. Umari and A. Pasquarello, Diam. Relat. Mater. **14**, 1255 (2005).
[23] F. L. Galeener, G. Lucovsky, and C. Mikkelsen, Jr., Phys. Rev. B **22**, 3983 (1980).
[24] A. Pasquarello and R. Car, Phys. Rev. Lett. **79**, 1766 (1997).
[25] A. Pasquarello and R. Car, Phys. Rev. Lett. **80**, 5145 (1998).
[26] P. Umari, A. Pasquarello, and A. Dal Corso, Phys. Rev. B **63**, 094305 (2001).
[27] $N_{\mathrm{O,boroxol}}/N_{\mathrm{tot}} = 2f/5$; $N_{\mathrm{O,nonboroxol}}/N_{\mathrm{tot}} = 3/5 - 2f/5$.
[28] D. Sebastiani and M. Parrinello, J. Phys. Chem. A **105**, 1951 (2001); We used the CPMD code [32] with normconserving pseudopotentials for B and O atoms and an energy cutoff of 70 Ry for the plane-wave basis set.
[29] J. V. Smith and C. S. Blackwell, Nature (London) **303**, 223 (1983); F. Mauri *et al.*, Phys. Rev. B **62**, R4786 (2000).
[30] S. K. Lee *et al.*, Phys. Rev. Lett. **94**, 165507 (2005).
[31] A. Pasquarello, Phys. Rev. B **61**, 3951 (2000).
[32] Computer code CPMD V3.7, copyright IBM Corp. 1990-2003; copyright MPI fuer Festkoerperforschung Stuttgart, 1997-2001. http://www.cpmd.org.